Volume 13
Number 34
14 September 2021
Pages 14257-14574

Nanoscale

rsc.li/nanoscale

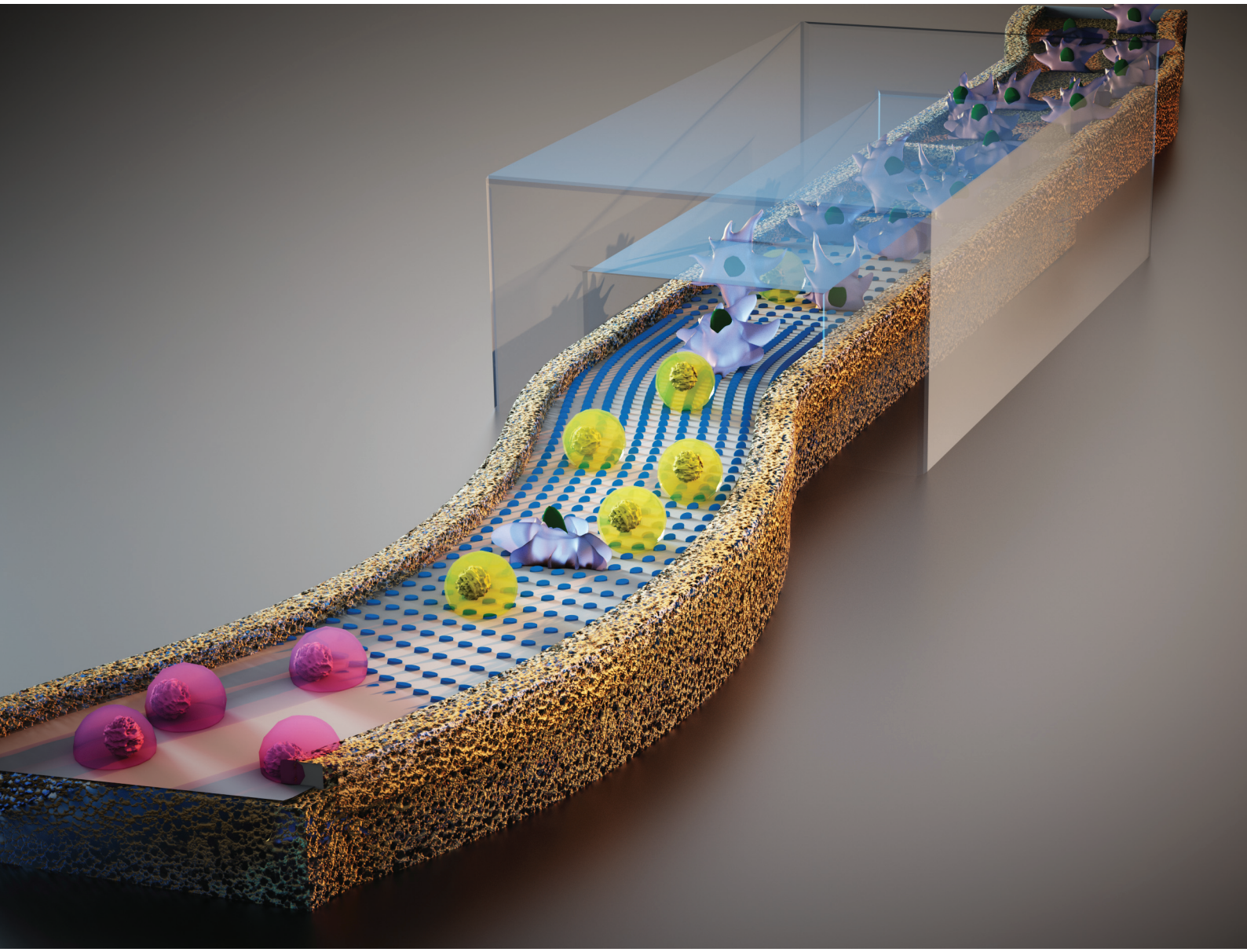

ISSN 2040-3372

ROYAL SOCIETY OF CHEMISTRY

PAPER
M. Nouri-Goushki, L. E. Fratila-Apachitei *et al.*
3D printed submicron patterns orchestrate the response of macrophages

NCNST

Nanoscale

PAPER

View Article Online
View Journal | View Issue

Cite this: *Nanoscale*, 2021, **13**, 14304

3D printed submicron patterns orchestrate the response of macrophages

M. Nouri-Goushki, *†[a] A. Isaakidou,†[a] B. I. M. Eijkel, [a] M. Minneboo,[a] Q. Liu,[b] P. E. Boukany,[b] M. J. Mirzaali,[a] L. E. Fratila-Apachitei*[a] and A. A. Zadpoor [a]

The surface topography of engineered extracellular matrices is one of the most important physical cues regulating the phenotypic polarization of macrophages. However, not much is known about the ways through which submicron (*i.e.*, 100–1000 nm) topographies modulate the polarization of macrophages. In the context of bone tissue regeneration, it is well established that this range of topographies stimulates the osteogenic differentiation of stem cells. Since the immune response affects the bone tissue regeneration process, the immunomodulatory consequences of submicron patterns should be studied prior to their clinical application. Here, we 3D printed submicron pillars (using two-photon polymerization technique) with different heights and interspacings to perform the first ever systematic study of such effects. Among the studied patterns, the highest degree of elongation was observed for the cells cultured on those with the tallest and densest pillars. After 3 days of culture with inflammatory stimuli (LPS/IFN-γ), sparsely decorated surfaces inhibited the expression of the pro-inflammatory cellular marker CCR7 as compared to day 1 and to the other patterns. Furthermore, sufficiently tall pillars polarized the M1 macrophages towards a pro-healing (M2) phenotype, as suggested by the expression of CD206 within the first 3 days. As some of the studied patterns are known to be osteogenic, the osteoimmunomodulatory capacity of the patterns should be further studied to optimize their bone tissue regeneration performance.

Received 10th March 2021,
Accepted 16th June 2021

DOI: 10.1039/d1nr01557e

rsc.li/nanoscale

1. Introduction

The successful integration of the biomaterials within their host tissues is mediated by immune responses.[1,2] The core regulators of the immune responses are macrophages, which play a major role in host defense and bone tissue healing.[3,4] The behavior of these cells is known to be modulated by soluble factors existing in the microenvironment of the host tissue.[5] In the presence of inflammatory substances, macrophages are activated towards their pro-inflammatory (M1) phenotype to defend the host against pathogens and inflammation.[6] In contrast, pro-healing factors actuate the M2 phenotype by expressing wound healing cytokines, contributing to tissue repair.[7] While the effects of soluble factors on macrophage polarization have been studied before, the mechanisms through which the physical cues of biomaterials influence macrophage polarization remain largely elusive.[8]

Among physical cues, those associated with the surface topography of implants are known to be capable of eliciting a favorable immune response.[9,10] Other studies have shown that the features of implant surfaces affect the trade-off between M1/M2 phenotypic polarization at the early stages of bone formation.[11,12] Topographies that prolonged the expression of the M1 cytokines caused chronic inflammation while a timely switch to the M2 phenotype promoted the osseointegration of the implant.[11–15] Recent studies suggest that submicron and nanoscale topographies could better regulate the pro-healing response than microscale topographies[16–18] since the size of the receptor of cells is in the nanoscale range.[19] However, the role of the dimensions of submicron (100–1000 nm) features on the polarization states of macrophages remains poorly understood. That is partially due to the difficulties associated with the fabrication of surfaces with precise micro-/nanoscale surface ornaments. Advanced micro- and nanofabrication techniques, such as 3D nanoprinting (*e.g.*, two-photon polymerization (2PP),[20,21] electron beam induced deposition

[a]*Department of Biomechanical Engineering, Faculty of Mechanical, Maritime, and Materials Engineering, Delft University of Technology (TU Delft), Mekelweg 2, 2628 CD Delft, The Netherlands. E-mail: m.nourigoushki@tudelft.nl, mhd.nouri71@gmail.com, E.L.Fratila-Apachitei@tudelft.nl*
[b]*Department of Chemical Engineering, Delft University of Technology (TU Delft), van der Maasweg 9, 2629 HZ Delft, The Netherlands*
† Joint first authors.

(EBID)[22]), and lithography-based techniques (*e.g.*, electron beam lithography (EBL),[23] nanoimprint lithography (NIL),[24] and focused ion beam lithography (FIBL)[25]), that have been relatively recently applied for biomedical applications,[1] have offered a path forward.

The study of the effects of submicron and nanoscale topographies on modulating the immune response is often performed with the ultimate aim of enhancing osteogenesis.[26,27] The osteoimmune response triggered by disordered patterns,[28] pores,[29] tubular motifs,[30] and groove-like[31] features have, therefore, been investigated both *in vivo*[30] and *in vitro.*[28,29,31] For example, titanium implants covered with semispherical nanoprotrusions (diameter: 80 nm, interspacing: 165 nm) fabricated by colloidal lithography are found to hinder the initial inflammatory cytokines and enhance the osteogenic response *in vivo.*[32] However, there is still a lack of information on whether pillar arrays in the submicron range (*i.e.*, 100 nm–1000 nm) promote osteoimmune responses. In fact, submicron pillars with a diameter of 200–300 nm and an interspacing of 450–700 nm (fabricated by NIL and 2PP) are shown to upregulate the osteogenic response of human adipose-derived stem cells (hADSCs) *in vivo*[33] and preosteoblast cells *in vitro*[34] without any osteogenic supplements. However, systematic studies that reveal the effects of the design parameters of submicron patterns on the immune response they elicit remain unavailable.

Here, we used an advanced 3D nanoprinting technique (*i.e.*, two-photon polymerization) to comprehensively study the effects of the height and spacing of submicron pillars on the immune response they cause. The cytokines secreted by a variety of cells in response to infection or tissue damage[35] can influence the response of macrophages and activate certain signaling pathways.[35,36] The role of such cytokines in modulating the (osteo)immune response triggered by submicron patterns have not been studied before. To bridge this knowledge gap, we investigated the morphology and polarization of murine-derived macrophages interacting with 6 different types of submicron patterns in the presence of M1-inducing stimuli at multiple time points. Moreover, we explored whether the proposed submicron pillars dimensions can modulate the polarization of M1 macrophages towards a more favorable pro-healing phenotype. This study was performed to examine the immunomodulatory potential of the osteogenic pillars that we have reported recently,[34] thereby portraying a more complete picture of the osteoimmunomodulatory potential of submicron patterns.

2. Materials and methods

2.1. Fabrication of the patterns

Six different patterns of submicron pillars (diameter = 250 nm, heights = 250, 500, 1000 nm, and interspacings = 700, 1000 nm) were designed in a computer aided design (CAD) program and were imported into Photonic Professional GT machine (Nanoscribe, Germany) according to a previously described method.[21] A laser power of 14% and a scanning speed of 1200 μm s^{-1} were applied to print the patterns atop a borosilicate coverslip substrate (Thermo Fisher Scientific, US) using the IP-L780 resin (Nanoscribe, Germany). The samples were then developed for 25 min in propylene glycol monomethyl ether acetate (PGMEA) (Sigma-Aldrich, Germany), rinsed with isopropyl alcohol (IPA) (Sigma-Aldrich, Germany) for 5 min, and dried with an air-blowing gun. We categorized the patterns (with a printed area of 500 × 500 μm^2) into two groups (*i.e.*, "S" and "L"). The interspaces between the pillars in groups S and L were 700 nm and 1000 nm, respectively. Each group contained patterns with 3 different heights (*i.e.*, S1 (or L1) = 250 nm, S2 (or L2) = 500 nm, S3 (or L3) = 1000 nm). In all experiments, we used a non-patterned borosilicate coverslip substrate as the control group.

2.2. Characterization of the patterns

The homogeneity of the patterns was evaluated with an optical microscope (Keyence Digital Microscope VHX-6000, USA). The histograms of the optical images of the printed areas were extracted using ImageJ (http://rsb.info.nih.gov/ij/index.html). The coefficient of variation (CV) of pixel intensity, which is defined as the standard deviation divided by the mean pixel intensity for each histogram was calculated to evaluate the uniformity of the patterns. A full geometrical characterization of the patterns was performed using scanning electron microscopy (SEM) (Helios Nano Lab 650, FEI, USA). The specimens were gold-sputtered (coating thickness ≈ 5 nm) using a gold-coater (JFC-1300, JEOL, Japan). The images of the specimens were acquired with a tilt angle of 30°. The images were further processed in ImageJ to determine the height and diameter of the pillars (36–45 pillars originating from 3 different samples were analyzed for each pattern type).

2.3. Cell experiments

2.3.1. Cell culture conditions. A concentration of 7 × 10^5 cells per mL murine macrophages (at passage 15, J774A.1, Merck KGaA, Germany) were cultured in 75 cm^2 flasks (Greiner Bio-One GmbH, Austria) with 20 mL of the Dulbecco's Modified Eagle's medium (DMEM: 10% (v/v) fetal bovine serum and 1% of penicillin–streptomycin (ThermoFisher Scientific, US)), and were incubated at 37 °C and 5.0% CO_2. After 3 days of culture, the cells were centrifuged and seeded onto the experimental substrates at a concentration of 5 × 10^4 cells per mL. The medium was refreshed every two to three days.

One day after the seeding of the cells onto the surfaces, the morphologies of the cells residing on the substrate were investigated with SEM. Towards that end, the DMEM culture medium was discarded, the specimens were rinsed twice with phosphate-buffered saline (PBS), and were consequently fixed in a 4% (v/v) formaldehyde/PBS solution (PFA, Sigma-Aldrich, Germany) at room temperature for 15 min. The specimens were then rinsed with distilled water for 5 min and were incubated with 50%, 70%, and 96% ethanol (Sigma-Aldrich, Germany) solutions for 15 min, 20 min, and 20 min, respect-

ively. The specimens were then allowed to dry overnight at room temperature, were gold-sputtered for 40 s, and were imaged with SEM.

2.3.2. Cell viability. The viability of macrophages was investigated using a live/dead assay (ThermoFisher Scientific, US). After 48 h of seeding, the cells were rinsed with PBS 10×, PBS 1×, and were incubated in a mixture of 0.1 μL mL^{-1} Calcein acetoxymethyl (AM)/PBS, and 1.5 μL mL^{-1} Ethidium homodimer 1 (EthD-1)/PBS. After 30 min, the solution was replaced with PBS and the cells were imaged with a fluorescent microscope (ZOE Fluorescent Cell Imager, BioRad, US). EthD-1 dye (in red) binds to the DNA of the cells with a disrupted membrane, while calcein AM binds to the cellular membrane and can be transported inside living cells where it becomes green fluorescent after the acetoxymethyl is hydrolyzed by intracellular esterases (according to the Thermofisher guideline).

2.3.3. Seeding cells on the patterns with inflammatory cytokines. The control groups and patterned substrates were first sterilized with 70% ethanol followed by rinsing with PBS. Next, a concentration of 5×10^4 cells per mL was seeded onto the samples, and the cells were incubated in DMEM (37 °C, 5% CO_2). After 6 h of incubation, a concentration of 100 ng mL^{-1} of lipopolysaccharide (LPS, Sigma-Aldrich, Germany) and 10 ng mL^{-1} of interferon gamma (IFN-γ, Sigma-Aldrich, Germany) were added to the culture medium. The samples were immunostained on days 1 and 3, followed by imaging with a confocal microscope (ZEISS LSM 900, Germany).

2.3.4. M1/M2 macrophages controls. A concentration of 5×10^5 cells per mL macrophages (at passage 15) were cultured in 6-well plate on control samples and were incubated at 37 °C, 5% CO_2 in DMEM. The medium was refreshed after 3 days. The cells were stimulated towards the M1 phenotype through the addition of 100 ng mL^{-1} LPS and 10 ng mL^{-1} of IFN-γ to the culture medium for 72 h. For the M2 stimulation, the same cell seeding procedure was performed and 10 ng mL^{-1} of IL-4 (Sigma-Aldrich, Germany) was added to the culture medium for 72 h before immunostaining analysis.

2.3.5. Immunoassay of IL-10. The expression of mouse interleukin 10 (IL-10) by M0, M1 and M2 cells was measured using a Victor X3 microplate reader (PerkinElmer, Groningen, The Netherlands). We followed the protocol provided by Abcam company (SimpleStep ELISA kit, Abcam, UK). Briefly, after centrifugation, the culture media of (non)activated cells was diluted with a 50× cell extraction enhancer solution to reach a 1× solution. 50 μL of the 1× supernatant was then incubated with 50 μL mixture of mouse IL-10 antibodies ("Capture" and "Detector") for 1 h at room temperature. Thereafter, the wells were washed three times with 340 μL of 1x wash buffer (PT, abcam, UK), 100 μL development solution was then added to each well and incubated on a plate shaker (400 rpm) at room temperature. After 10 min, 100 μL of "Stop" solution was added to each well and the optical density (OD) was measured at 450 nm.

2.3.6. Griess assay of NO. The secretion of nitric oxide (NO) was measured according to the protocol provided in the Griess reagent kit (Abcam, US). Briefly, the culture media of (non)activated cells was collected and centrifuged for 5 min. 100 μL of the supernatant was added to each well and then mixed with 100 μL of a "reaction" solution. The microplate was incubated for 10 min at room temperature. Then, the absorbance of the wells was read at the wavelength of 540 nm using the same Victor X3 microplate reader.

2.3.7. Culturing of M1 stimulated macrophages on the patterns. A similar M1 stimulation protocol (described above) was performed in 75 cm^2 flasks. A concentration of 7×10^5 cells per mL macrophages (at passage 15) were cultured in flasks with 20 mL of DMEM and were incubated at 37 °C, 5% CO_2, followed by the addition of 100 ng mL^{-1} of LPS and 10 ng mL^{-1} of IFN-γ to the culture medium and incubation for another 72 h. Three days before immunostaining, the M1 stimulated cells were seeded on the patterned and control specimens at a concentration of 5×10^5 cells per mL.

2.3.8. Immunofluorescence imaging. The specimens were washed twice with PBS and were then fixed with a 4% (v/v) formaldehyde solution for 15 min at room temperature. After another washing step with PBS, the macrophages were permeabilized through the addition of 0.5% Triton/PBS (Sigma-Aldrich, Germany) for 15 min at 4 °C. The membrane of the cells was blocked with 1% bovine serum albumin (BSA)/PBS (Sigma-Aldrich, Germany) for 5 min at 37 °C. Next, the specimens were overnight incubated (at 4 °C) in a mixture of the primary antibodies C–C chemokine receptor type 7 (CCR7) and the macrophage mannose receptor (CD206) (both 1 : 100 in 1% BSA/PBS, Abcam, UK). After 3 times of rinsing with 0.5% Tween/PBS, the samples were incubated in the secondary antibodies Alexa-Fluor 488 (1 : 50 in 1% BSA/PBS, ThermoFisher Scientific, US) and Alexa-Fluor 594 (1 : 150 in 1% BSA/PBS, ThermoFisher Scientific, US) for 1 h at room temperature. Finally, the specimens were washed with PBS and were mounted on microscope glass slides with 10 μL of Prolong gold (containing 4′,6-diamidino-2-phenylindole (DAPI), Life Technologies, USA). The imaging of stained cells was performed using a confocal microscope (ZEISS LSM 900, Germany).

2.3.9. Image analysis. We used ImageJ to analyze the cell area, degree of elongation (*DE*), and expression levels of the biomarkers. The fluorescent images were split into single-colored channels, and the grayscale images were analyzed to quantify the data, as described in our previous studies.[21,34] Here, *DE* was calculated as the ratio of the major to the minor axes of the ellipse fitted to single cells. Between 86–303 cells were analyzed per experimental group ($n = 4$). The mean fluorescent intensity of the biomarkers was quantified for at least 15 cells on day 1 and 50 cells on day 3 within a fixed area of 500 × 500 μm^2. Cell clusters were neglected in all evaluations.

2.3.10. Statistical analysis. The data are presented as mean ± standard deviation (SD). Depending on the number of the experimental groups being compared, either the Wilcoxon test or one-way ANOVA followed by the Tukey's *post-hoc* analysis were used (software: R (https://www.r-project.org), significance threshold: $p < 0.05$).

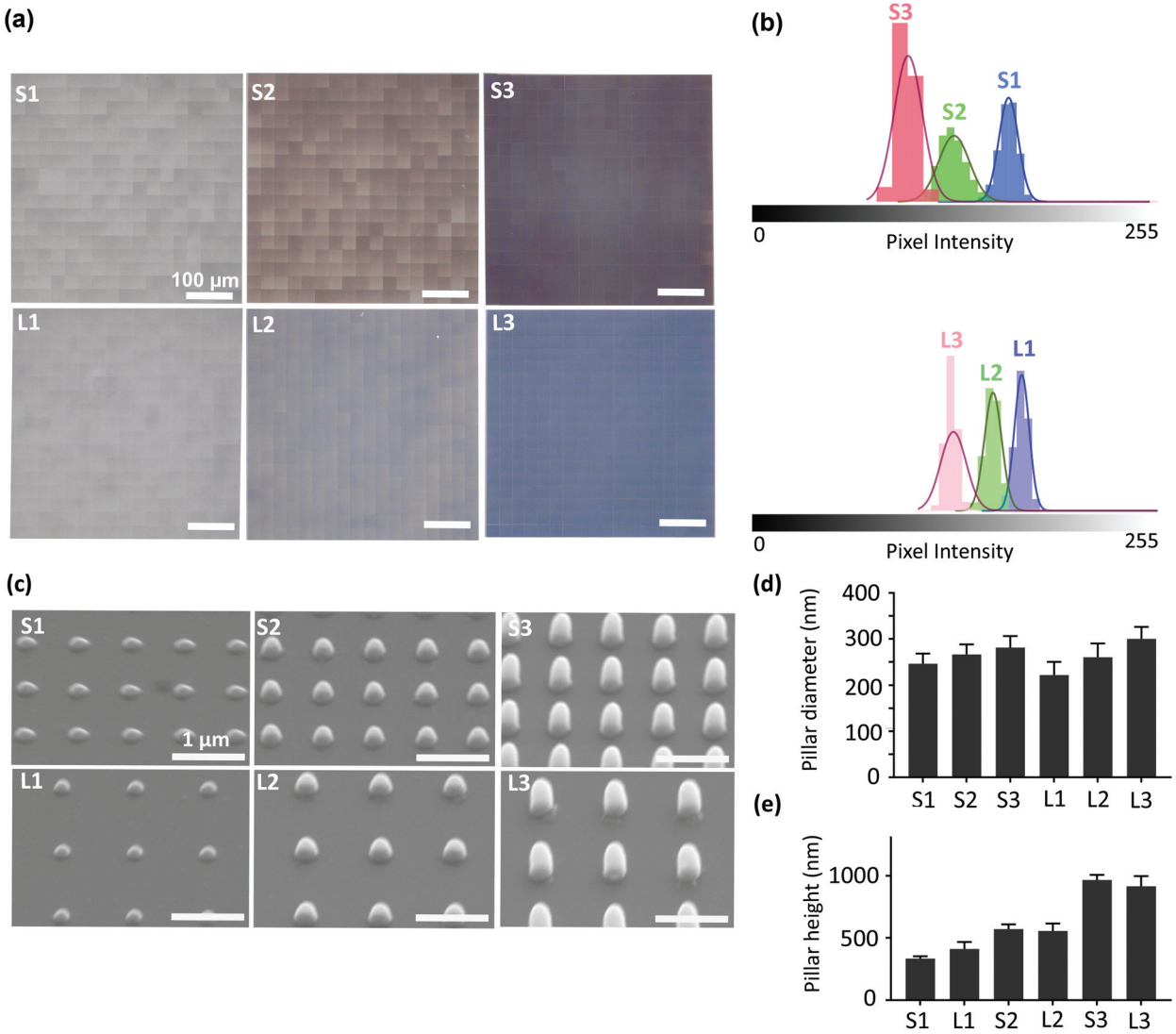

Fig. 1 The characterization of the submicron pillars. (a) The optical microscopy images of the patterned area showing the uniformity of the printed pillars. (b) The histograms of the pixel intensity values obtained from the optical images. (c) The SEM images of the 6 different types of patterns studied here. (d) The quantified values of the diameter and (e) height of the pillars.

3. Results

3.1. Characterization of the patterns

3.1.1. Microscopic characterization. The microscopic visualization of the patterned surfaces showed different pixel intensities among specimens (Fig. 1a and b). The mean pixel intensity of the patterned areas decreased as the height and density of the pillars increased (Fig. 1b and Table 1), leading to darker images. The CV was < 10% for all the patterned surfaces (Table 1), indicating the high accuracy and uniformity of the printed pillars. The dimensions of the pillars were quantified by analyzing the captured SEM images (Fig. 1c, d and e). A slight variation (SD ≈ 24 nm) in the diameter of the pillars was observed as compared to the designed value (250 nm) (Fig. 1d), which could be attributed to the slight fluctuations in the laser power that the resin receives during the printing process. This laser power fluctuation led to a slight variation in the height of the pillars compared to the design value (Fig. 1e).

Table 1 The uniformity of the printed area is reported by the mean and coefficient of variation (CV) in the pixel intensity of the optical images

Groups	Mean pixel intensity	CV (%)
S1	165 ± 6	4
S2	130 ± 10	8
S3	100 ± 9	9
L1	168 ± 5	3
L2	150 ± 6	4
L3	124 ± 8	7

3.1.2. Cytocompatibility. The live/dead fluorescence microscopy images of the J774A.1 macrophages cultured on the control (non-patterned substrate) and patterned surfaces (S2) (Fig. 2a and b) showed that the cells were alive after 48 h of culture on both control and patterned surfaces. Moreover,

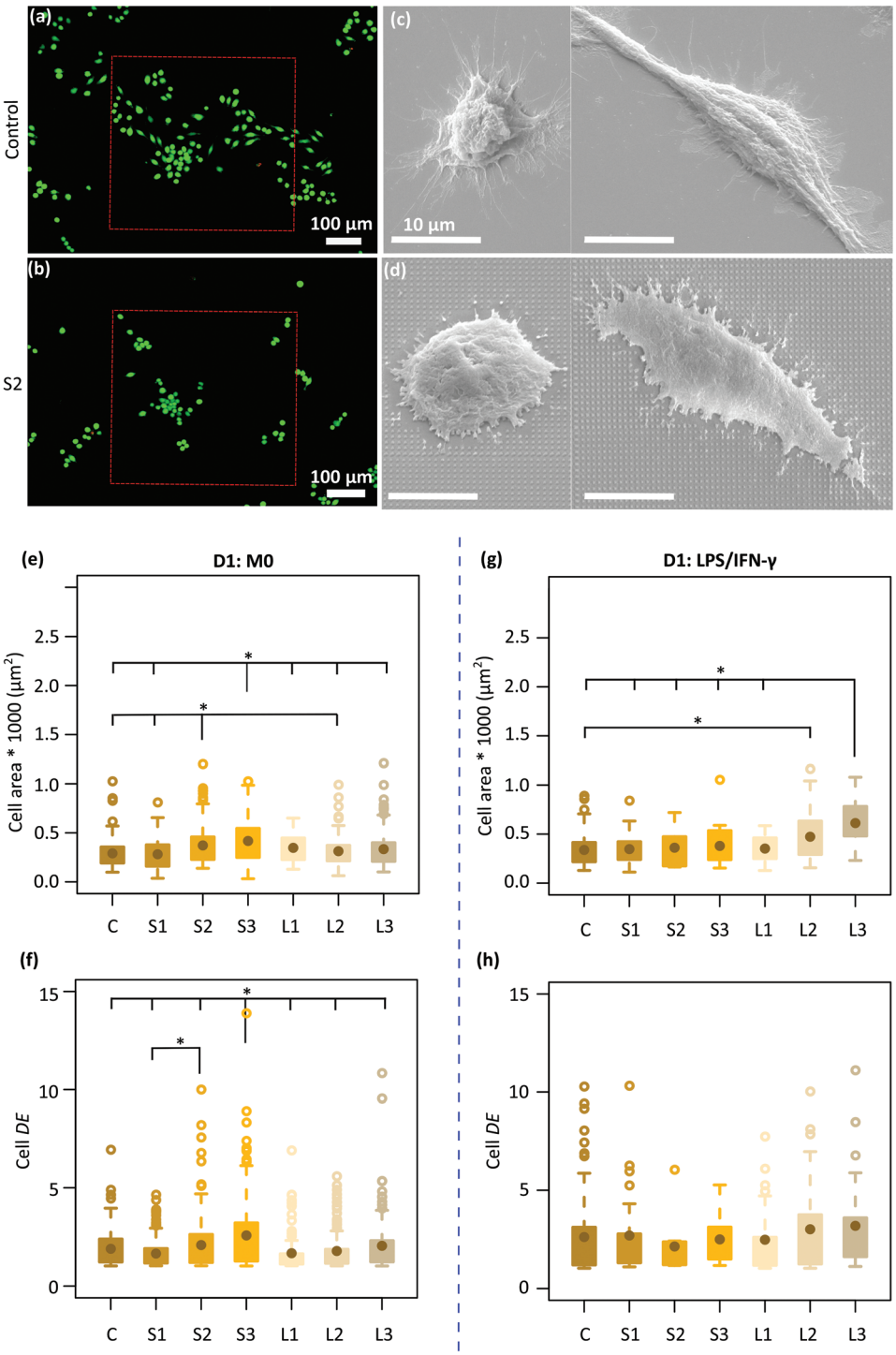

Fig. 2 Cell viability and morphology on the patterned surfaces. The live/dead staining of J774A.1 cells after 2 days of culture on the (a) control and (b) a representative patterned specimen (S2). The SEM images of the cell-surface interaction: the different types of cell morphology (M0) observed after 1 day on (c) a control specimen and (d) a representative patterned surface (S2). The quantification area of (e) non-treated and (g) LPS/IFN-γ treated cells residing on the control and patterned surfaces after 1 day of culture. The quantification of cell elongation (*DE*) for (f) non-treated and (h) LPS/IFN-γ treated macrophages on the control and patterned surfaces after 1 day of culture (*$p < 0.05$).

the cells migrated close to the center and edges of the patterned area, showing the cellular interaction and migration of cells on the patterns and confirming the cytocompatibility of the IP-L780 material for this specific cell type.

3.2. Macrophages morphology on submicron pillars with (out) inflammatory cytokines

Two types of macrophage shapes (*i.e.*, round and polarized) were observed on both the control and patterned surfaces after 1 day of culture (Fig. 2c and d) in the absence of inflammatory cytokines. Furthermore, on the control specimens, the cells appeared well-spread with numerous long cytoplasmic extensions (Fig. 2c) whereas on the patterned surfaces, they were shrunk, with short membrane protrusions attached to the pillars, indicative of a more tense state (Fig. 2d). The average area of the cells residing on the different types of specimens was around 281–417 μm^2. Furthermore, the largest cells with an average area of $\approx$ 400 μm^2 were mainly observed on the denser pillars (S2, S3) (Fig. 2e). The *DE* of the cells cultured on different patterned surfaces was between 1.6–2.6. Within 1 day, the cells residing on the tallest and densest pillars (S3) appeared to be significantly more elongated (*DE* $\approx$ 2.6) as compared to the cells present on the other types of patterned and control surfaces (Fig. 2f).

In the presence of M1 stimulators, the same mix of cell shapes, namely round and polarized, were observed on all the patterns and the control surfaces. Also, no difference in cell area and degree of elongation was observed between different patterns (Fig. 2g and h). However, the area of the cells residing on the L2 (473 $\pm$ 256 μm^2) and L3 (612.5 $\pm$ 225 μm^2) patterns was significantly higher as compared with the area of the cells on the control specimens (338 $\pm$ 157 μm^2) (Fig. 2g).

3.3. Macrophage polarization on submicron pillars

We first analyzed the effect of cytokines, LPS/IFN-γ (for M1 phenotype), and IL-4 (for M2 phenotype) on the polarization and morphology of macrophages cultured on the control specimens (Fig. 3a–f). After three days, the activation of M1 cells was examined by a pro-inflammatory (M1) surface marker, CCR7 and secretion of NO (Fig. 3a and b). A considerable amount of NO was expressed by M1 cells (Fig. 3b), showing the presence of an inflammatory microenvironment.[37] On the other hand, the orange color in M2 cells (Fig. 3a) showed both CCR7 and CD206 markers (the latter being representative of pro-healing (M2) phenotype). To check the activation of M2 cells, we have measured the expression of an M2-prohealing cytokine, interleukin-10 (IL-10). IL-10 was significantly upregulated in the M2 cells (Fig. 3c), indicating the anti-inflammatory microenvironment.[38] After 3 days of stimulation, the morphology of the cells stimulated to the M1 phenotype (referred to as the M1 cells) was markedly different from that of the cells stimulated to the M2 phenotype (referred to as the M2 cells) (Fig. 3a, d and e). M1 cells exhibited an elongated (*DE* $\approx$ 3.3 $\pm$ 2) and spread morphology with a significantly larger area ($\approx$ 3133 $\pm$ 1667 μm^2) (Fig. 3a, d and e) than the M2 cells, which were rounder (*DE* $\approx$ 1.8 $\pm$ 0.8) and smaller in area ($\approx$ 398 $\pm$ 157 μm^2) (Fig. 3a, d and e). The polarization state of the cells on the flat control surfaces was evaluated on day 1 and day 3 using the CCR7 and CD206 surface markers (Fig. 3f). The cells stimulated with LPS/IFN-γ secreted noticeably higher levels of CCR7 on day 3 as compared to day 1 (Fig. 3f). However, the expression of CD206 was relatively low on both days and did not change over time (Fig. 3f).

After 1 day of cell culture on the patterned surfaces without any inflammatory cytokines, the expression of CCR7 was significantly enhanced with the height of the pillars but not with their interspacing, indicating that pillars taller than 500 nm (S2, S3, L2, L3) tend to stimulate the pro-inflammatory phenotype (Fig. 3g). In comparison, the expression of CD206 remained at the same level on the various patterned surfaces and was lower than the control specimens (Fig. 3j). By the addition of the LPS/IFN-γ to the culture medium, both markers seem to be downregulated after day 1 (Fig. 3h and k). When comparing different patterns, for CCR7 (Fig. 3h), the effects of pillar height was still present but the interspacing also showed an effect on the expression of CCR7. More specifically, the taller pillars with a larger interspacing (L2, L3) significantly promoted the expression of CCR7 relative to the corresponding denser patterns (S2, S3), indicating a pro-inflammatory response induced by these patterns in the presence of inflammatory stimuli (Fig. 3h).

Increasing the time of cell culture to 3 days in the presence of LPS/IFN-γ (Fig. 3i and l) changed the expression levels of the two markers. Thus, for the CCR7 the trend reversed as the levels increased on S1-S3 patterns relative to day 1 while on L1–L3 patterns the levels were not really changing with time. This finding indicates the potential of the L1–L3 patterns to inhibit the M1 polarization of macrophages with time (Fig. 3i). In such an inflammatory environment, an insignificant difference in the amount of CD206 was observed between cells that resided on different submicron pillars (Fig. 3l). A statistically significant difference was only observed between L1 and S1 patterns (Fig. 3l).

In summary, during the 3 days of culture in medium containing pro-inflammatory stimuli (LPS/IFN-γ) the pillars with a height of 500 and 1000 nm, and an interspacing of 1000 nm (L2, L3) inhibited the expression of CCR7 M1 marker and promoted the M2 CD206 marker by the macrophages. By comparison, the corresponding denser patterns (S2 and S3) stimulated the expression of both markers during the 3 days of culture.

3.4. Morphology and polarization of M1 macrophages on submicron pillars

To better delineate the effects of the patterns on macrophage polarization, the starting cells were first stimulated to M1 and then cultured on the patterns and the control surfaces for 3 days (Fig. 4a). The average area of the cells cultured on the patterned surfaces and control specimens was in the range of 280–560 μm^2 (Fig. 4b). Furthermore, a wider distribution of the cell area was observed on the patterns with a larger interspace (L series) (Fig. 4b). Moreover, the average *DE* of the cells residing on different patterned surfaces and control samples

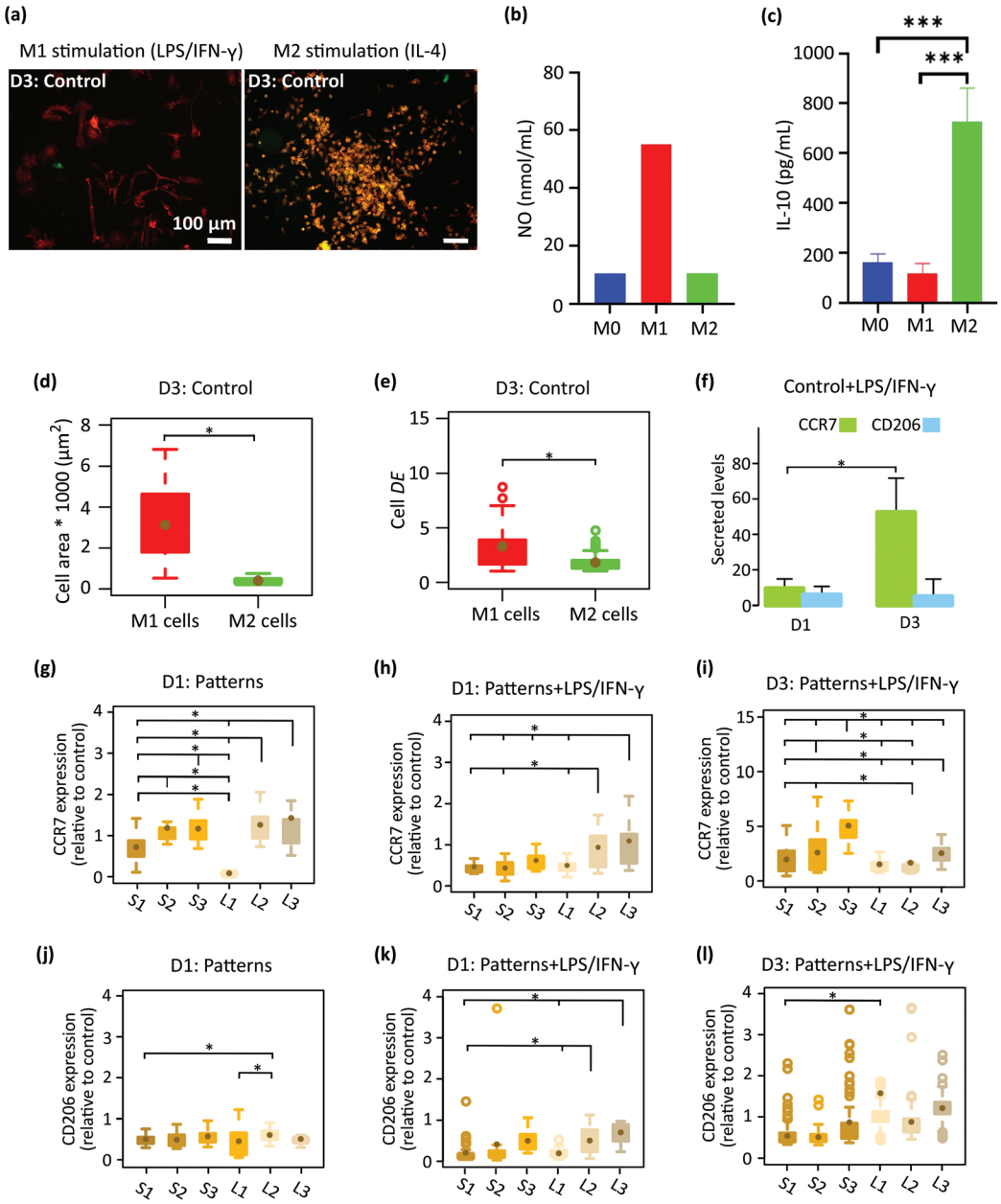

Fig. 3 (a) The immunofluorescent images of LPS/IFN-γ and IL-4 treated macrophages stained for CCR7 (M1 phenotype in red) and CD206 (M2 phenotype in green) after 3 days of culture on the control substrate. (b and c) Expression of NO and IL-10 in M0, M1, and M2 activated cells. (d) The area and (e) elongation degree (*DE*) of M1 and M2 stimulated cells after 3 days of culture on the control surface. (f) Secreted markers in LPS/IFN-γ treated cells after 1 and 3 days of culture on the control surface. The expression level of (g) CCR7 and (j) CD206 in macrophages cultured on the patterned surfaces for 1 day (relative to cells cultured on the control surface). (h and i) The expression level of CCR7 and (k and l) CD206 in LPS/IFN-γ treated cells cultured on the patterned surfaces for 1 and 3 days, respectively (relative to cells residing on the control surface) (*$p < 0.05$).

was in the same range (*i.e.*, 1.4–2), indicating two types of cell shapes (*i.e.*, round and polarized) on the different surfaces (Fig. 4c). Furthermore, both surface phenotype markers (*i.e.*, CCR7 and CD206) were expressed in both populations: CCR7 (in red) was observed at the boundary of the cells while CD206 (in green) was detected at the center of the cells and around the nucleus (Fig. 4a). The fluorescence signal of CCR7 remained similar across all the experimental groups, which was almost twice as much as the control specimens (Fig. 4d). The expression of the M2 marker (CD206) was also upregulated in the macrophages cultured on all six types of patterned substrates as compared to the control specimens but more differences were observed between the various patterns. The height of the pillars was correlated with the levels of the CD206 expression by the cells cultured on the densely patterned surfaces (*i.e.*, S series). The interspacing of the higher pillars did not change the expression level of CD206 (Fig. 4e). For example, similar levels of CD206 expression were observed

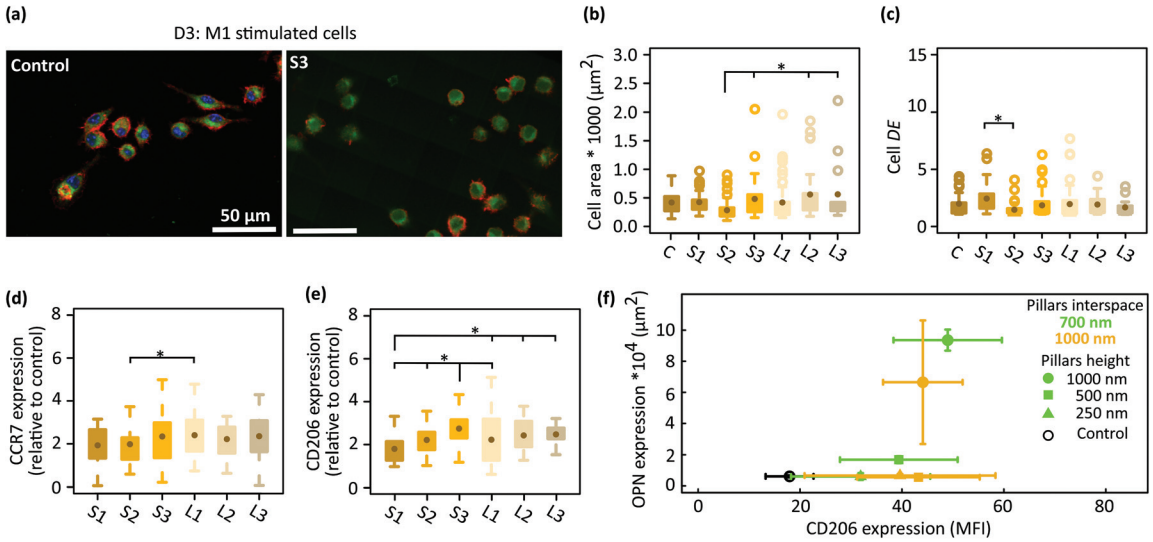

Fig. 4 (a) The fluorescent images of immunostained M1 stimulated macrophages for CCR7 (red) and CD206 (green) after 3 days of culture on the control and a representative pattern (S3). (b) The cell area and (c) degree of elongation (*DE*) of the M1 cells cultured on patterned and control surfaces. The expression level of (d) CCR7 and (e) CD206 in the M1 cells cultured on patterned surfaces for 3 days (relative to the control surfaces). (f) The expression of OPN in preosteoblasts after 21 days of culture on the patterns[32] and that of CD206 in M1 cells residing on the patterned surfaces for 3 days. The mean fluorescence intensity (MFI) of the CD206 is reported (*$p < 0.05$).

on (S2 and L2) and (S3 and L3). In summary, these results indicated that the patterns modulated the polarization of M1 macrophages after 3 days of culture and that the effective sizes for the height and interspacing of submicron pillars to promote the polarization of M1 macrophages towards a pro-healing M2 phenotype are 500 and 1000 nm, and 700 and 1000 nm, respectively.

4. Discussion

In the *in vivo* microenvironment of tissues, cytokines can be secreted naturally by a variety of cells in response to infection or cellular damage.[35] For example, the type II activated murine macrophages secrets IL-4,[39] and human macrophages produces IFN-γ.[40] These cytokines are known to manipulate the macrophages morphology and activation through binding to cell receptors and consequently transducing signals to the nucleus.[35,36] Studying the role of submicron pillars on the macrophage phenotype in the presence of the critical cytokines mediators is of crucial importance and has not been investigated before.

Although the effects of surface topography on the behavior of macrophages have been extensively studied in the literature, there is limited information on how surface topographies modulate both the osteogenic and immune responses. Most current topographies are being assessed only for one cell type, either immune[11,15,18] or osteogenic.[19] A potent physical cue should be capable of modulating immunogenic response without affecting the osteogenic activity but rather promoting it. In the context of osteoimmunomodulatory biomaterials, mainly macrophage conditioned medium was used for osteoblasts differentiation.[41] However, both macrophages and osteoblast are in direct contact with the biomaterials *in vivo*.

We systematically studied the role of the design parameters of 3D printed submicron pillars on the morphology and polarization of macrophages in different testing conditions: (1) in the presence of inflammatory stimuli added in the medium and (2) using M1 phenotype cells. When macrophages were cultured with LPS/IFN-γ (inflammatory stimuli) on the control specimens, a longer culture time (3 days) was required for an effective polarization towards M1 (a pro-inflammatory response) (Fig. 3f). Moreover, the M1 phenotype was associated with a highly elongated and more spread shape, which is in line with the observations reported in previous studies.[42] The same transition time point (*i.e.*, 3 days) was observed for the cells cultured on submicron pillars in the presence of LPS/IFN-γ. In this condition, cells residing on the shortest pillars (L1) expressed higher CD206 relatively to the ones settling on the corresponding pattern with smaller interspace (S1) (Fig. 3l). Although the expression of CD206 on the other patterns did not change significantly after 3 days of culture with LPS/IFN-γ (Fig. 3l), the pillars with a larger interspacing (*i.e.*, L series) inhibited the secretion of the M1 marker in the presence of inflammatory stimuli (Fig. 3i). Interestingly, when M1 macrophages were cultured on submicron pillars (Fig. 4), the polarization towards the M2 phenotype was stimulated by the tallest pillars (S3, L3) (Fig. 4e), while no visible changes in the area and elongation of the cells residing on different patterned surfaces were observed (Fig. 4b, c). A possible reason might be the increase in the surface hydrophilicity with increasing the height of the pillars which we observed in our previous study.[34] Surface hydrophilicity steers the polarization of the macrophages towards an anti-inflammatory response by

mediating the adsorption of fibronectin and fibrinogen proteins.[43] Macrophages adhered on a hydrophilic surface interact with the absorbed fibronectin through integrin β1 which in turn enhances the phosphorylation levels of phosphoinositide 3-kinase (PI3K) and serine/threonine kinase (Akt) and consequently enhances the secretion of anti-inflammatory cytokines and M2 surface markers (*e.g.*, CD206).[43,44]

In a previous study,[32] we evaluated the expression of OPN on the same 6 patterned surfaces. We found that taller and denser pillars (S3) stimulate the expression of OPN in both osteogenic and non-osteogenic conditions. Our results, here, reveal the role of interspacing in suppressing the pro-inflammatory phenotype of macrophages in the presence of LPS/IFN-γ (potent patterns: L2 and L3 patterns) as well as the role of the pillar height in promoting the polarization of M1 macrophages towards a pro-healing phenotype (potent patterns: S3, L3). Therefore, in the submicron range, sufficiently tall pillars could have osteoimmunomodulatory properties (Fig. 4f).

Among the multiple types of patterns[27,45–47] that were studied in terms of their osteo(immuno)modulatory properties, pillars with a diameter of 200–300 nm are reported to promote the expression of osteogenic factors.[33] We, previously,[34] showed that the same S3 patterns (pillars with a diameter in this range) promote the matrix mineralization of preosteoblasts by enhancing cell adhesion, regulating the cell shape, and modulating the mechanical properties of the cytoskeleton. Here, we found that those pillars also cause macrophages to shrink, indicative of intracellular tension, and to upregulate the pro-healing response of M1 macrophages. Regulating the polarization of macrophages is associated with tension and contraction in the cytoskeleton of the cells.[48] Cytoskeletal tension, as measured by the level of Rho-associated protein kinase (ROCK-activity), can lead to the upregulation of anti-inflammatory genes in macrophages.[48–50] The underlying mechanisms involve the elongation and tension in actin fibers directly affecting the organization of the nucleus and the condensation of chromatin that eventually influence the macrophage phenotype.[48]

Unraveling the role of ECM topographies in the polarization of macrophages has motivated researchers to use patterning techniques for the development of ECM-mimicking implant surfaces. The surface topography of implants influences the adhesive interactions,[51] cell morphology[52,53] and gene expression[54–56] of the cells that come into contact with them. The type and dimensions of surface features play a crucial role in modulating the response of both immune (*e.g.*, monocytes and macrophages)[57] and bone (*e.g.*, osteoblasts and osteoclasts) cells[58] existing in the tissue microenvironment. Submicron-nanofeatures are known to more effectively influence the response of cells as compared to microfeatures. That is often attributed to their size, which is closer to the cell receptors.[11,26] Given the fact that multiple cell types are present in the extracellular microenvironment and that they respond differently to topographies as well as existing cytokines in their surroundings, it is crucial to precisely control and carefully optimize the dimensions of micro-/nano-features present on implant surfaces.[26]

5. Conclusions

For the first time, we investigated the effects of the height (250–1000 nm) and interspacing (700 nm, 1000 nm) of 3D printed submicron pillars on the response of murine macrophages (J77A.1) in the presence of soluble inflammatory factors (LPS/IFN-γ). Driven by the advances in nanofabrication techniques, we produced submicron pillars with high accuracy in a single-step procedure. The cytocompatibility of the material from which the patterns were made was confirmed in our experiments. Both round and elongated cells were observed on the patterned and control surfaces. The M1-stimulated cells were significantly larger in their area and degree of elongation than the M2-stimulated cells. Furthermore, the proposed submicron pillars modulated the macrophage responses even in the presence of LPS/IFN-γ. In this condition, the patterns effects also changed over time: on day 1, pillars with a higher (lower) pillar density impeded (boosted) the expression of the pro-inflammatory marker, while opposite results were observed on day 3. Moreover, in the absence of inflammatory solubles, the tallest pillars with higher pillar densities encouraged a switch of M1 macrophages to the pro-healing M2 phenotype after 3 days and improved the osteogenic activity of preosteoblast cells. This work provides the basis for future exploration of the osteoimmunomodulatory phenomena that are associated with submicron topographies and are of relevance for the development of orthopedic implants.

Conflicts of interest

The authors declare that they have no competing interests.

Acknowledgements

The research leading to these results has received funding from the European Research Council under the ERC grant agreement no. [677575]. We would like to thank Prof. Dr. Urs Staufer (Department of Precision and Microsystems Engineering, TU Delft) for his comments on the manuscript, Dr. Daniel Fan (Department of Precision and Microsystems Engineering, TU Delft) for the technical assistance with the Nanoscribe equipment, and Dr. Cornelis W. Hagen (Department of Imaging Physics, TU Delft) for the access to the SEM equipment. Dr. Q. Liu. and Dr. P. E. Boukany acknowledge the funding from the European Research Council (ERC) under the European Union's Horizon 2020 research and innovation programme [grant agreement no. 819424].

References

1 G. Mendonça, D. B. S. Mendonça, F. J. L. Aragão and L. F. Cooper, Advancing dental implant surface technology – From micron- to nanotopography, *Biomaterials*, 2008, **29**(28), 3822–3835.

2 C. R. Arciola, D. Campoccia and L. Montanaro, Implant infections: adhesion, biofilm formation and immune evasion, *Nat. Rev. Microbiol.*, 2018, **16**(7), 397–409.

3 D. G. Russell, L. Huang and B. C. VanderVen, Immunometabolism at the interface between macrophages and pathogens, *Nat. Rev. Immunol.*, 2019, **19**(5), 291–304.

4 J. Pajarinen, T. Lin, E. Gibon, Y. Kohno, M. Maruyama, K. Nathan, L. Lu, Z. Yao and S. B. Goodman, Mesenchymal stem cell-macrophage crosstalk and bone healing, *Biomaterials*, 2019, **196**, 80–89.

5 L. Saldaña, F. Bensiamar, G. Vallés, F. J. Mancebo, E. García-Rey and N. Vilaboa, Immunoregulatory potential of mesenchymal stem cells following activation by macrophage-derived soluble factors, *Stem Cell Res. Ther.*, 2019, **10**(1), 58.

6 G. L. Seim, E. C. Britt, S. V. John, F. J. Yeo, A. R. Johnson, R. S. Eisenstein, D. J. Pagliarini and J. Fan, Two-stage metabolic remodelling in macrophages in response to lipopolysaccharide and interferon-γ stimulation, *Nat. Metab.*, 2019, **1**(7), 731–742.

7 D. Hachim, S. T. LoPresti, R. D. Rege, Y. Umeda, A. Iftikhar, A. L. Nolfi, C. D. Skillen and B. N. Brown, Distinct macrophage populations and phenotypes associated with IL-4 mediated immunomodulation at the host implant interface, *Biomater. Sci.*, 2020, **8**(20), 5751–5762.

8 Y. Jia, W. Yang, K. Zhang, S. Qiu, J. Xu, C. Wang and Y. Chai, Nanofiber arrangement regulates peripheral nerve regeneration through differential modulation of macrophage phenotypes, *Acta Biomater.*, 2019, **83**, 291–301.

9 S. Franz, S. Rammelt, D. Scharnweber and J. C. Simon, Immune responses to implants – A review of the implications for the design of immunomodulatory biomaterials, *Biomaterials*, 2011, **32**(28), 6692–6709.

10 H. Rostam, S. Singh, N. Vrana, M. Alexander and A. Ghaemmaghami, Impact of surface chemistry and topography on the function of antigen presenting cells, *Biomater. Sci.*, 2015, **3**(3), 424–441.

11 T. U. Luu, S. C. Gott, B. W. K. Woo, M. P. Rao and W. F. Liu, Micro- and Nanopatterned Topographical Cues for Regulating Macrophage Cell Shape and Phenotype, *ACS Appl. Mater. Interfaces*, 2015, **7**(51), 28665–28672.

12 E. Saino, M. L. Focarete, C. Gualandi, E. Emanuele, A. I. Cornaglia, M. Imbriani and L. Visai, Effect of Electrospun Fiber Diameter and Alignment on Macrophage Activation and Secretion of Proinflammatory Cytokines and Chemokines, *Biomacromolecules*, 2011, **12**(5), 1900–1911.

13 H. Cao, K. Mchugh, S. Y. Chew and J. M. Anderson, The topographical effect of electrospun nanofibrous scaffolds on the in vivo and in vitro foreign body reaction, *J. Biomed. Mater. Res., Part A*, 2010, **93**(3), 1151–1159.

14 K. Wang, W.-D. Hou, X. Wang, C. Han, I. Vuletic, N. Su, W.-X. Zhang, Q.-S. Ren, L. Chen and Y. Luo, Overcoming foreign-body reaction through nanotopography: Biocompatibility and immunoisolation properties of a nanofibrous membrane, *Biomaterials*, 2016, **102**, 249–258.

15 S. Chen, J. A. Jones, Y. Xu, H.-Y. Low, J. M. Anderson and K. W. Leong, Characterization of topographical effects on macrophage behavior in a foreign body response model, *Biomaterials*, 2010, **31**(13), 3479–3491.

16 C. Yang, C. Zhao, X. Wang, M. Shi, Y. Zhu, L. Jing, C. Wu and J. Chang, Stimulation of osteogenesis and angiogenesis by micro/nano hierarchical hydroxyapatite via macrophage immunomodulation, *Nanoscale*, 2019, **11**(38), 17699–17708.

17 V. Malheiro, F. Lehner, V. Dinca, P. Hoffmann and K. Maniura-Weber, Convex and concave micro-structured silicone controls the shape, but not the polarization state of human macrophages, *Biomater. Sci.*, 2016, **4**(11), 1562–1573.

18 S. Singh, D. Awuah, H. M. Rostam, R. D. Emes, N. K. Kandola, D. Onion, S. S. Htwe, B. Rajchagool, B.-H. Cha, D. Kim, P. J. Tighe, N. E. Vrana, A. Khademhosseini and A. Ghaemmaghami, Unbiased Analysis of the Impact of Micropatterned Biomaterials on Macrophage Behavior Provides Insights beyond Predefined Polarization States, *ACS Biomater. Sci. Eng.*, 2017, **3**(6), 969–978.

19 R. A. Gittens, T. McLachlan, R. Olivares-Navarrete, Y. Cai, S. Berner, R. Tannenbaum, Z. Schwartz, K. H. Sandhage and B. D. Boyan, The effects of combined micron-/submicron-scale surface roughness and nanoscale features on cell proliferation and differentiation, *Biomaterials*, 2011, **32**(13), 3395–3403.

20 M. Nouri-Goushki, A. Sharma, L. Sasso, S. Zhang, B. C. J. Van der Eerden, U. Staufer, L. E. Fratila-Apachitei and A. A. Zadpoor, Submicron Patterns-on-a-Chip: Fabrication of a Microfluidic Device Incorporating 3D Printed Surface Ornaments, *ACS Biomater. Sci. Eng.*, 2019, **5**(11), 6127–6136.

21 M. Nouri-Goushki, M. J. Mirzaali, L. Angeloni, D. Fan, M. Minneboo, M. K. Ghatkesar, U. Staufer, L. E. Fratila-Apachitei and A. A. Zadpoor, 3D Printing of Large Areas of Highly Ordered Submicron Patterns for Modulating Cell Behavior, *ACS Appl. Mater. Interfaces*, 2020, **12**(1), 200–208.

22 M. Ganjian, L. Angeloni, M. J. Mirzaali, K. Modaresifar, C. W. Hagen, M. K. Ghatkesar, P.-L. Hagedoorn, L. E. Fratila-Apachitei and A. A. Zadpoor, Quantitative mechanics of 3D printed nanopillars interacting with bacterial cells, *Nanoscale*, 2020, 21988–22001.

23 A. Klymov, L. Prodanov, E. Lamers, J. A. Jansen and X. F. Walboomers, Understanding the role of nano-topography on the surface of a bone-implant, *Biomater. Sci.*, 2013, **1**(2), 135–151.

24 L.-S. Wang, B. Duncan, R. Tang, Y.-W. Lee, B. Creran, S. G. Elci, J. Zhu, G. Yesilbag Tonga, J. Doble,

M. Fessenden, M. Bayat, S. Nonnenmann, R. W. Vachet and V. M. Rotello, Gradient and Patterned Protein Films Stabilized via Nanoimprint Lithography for Engineered Interactions with Cells, *ACS Appl. Mater. Interfaces*, 2017, **9**(1), 42–46.

25 T. Limongi, L. Tirinato, F. Pagliari, A. Giugni, M. Allione, G. Perozziello, P. Candeloro and E. Di Fabrizio, Fabrication and Applications of Micro/Nanostructured Devices for Tissue Engineering, *Nano-Micro Lett.*, 2016, **9**(1), 1.

26 T. M. Valentin, S. E. Leggett, P.-Y. Chen, J. K. Sodhi, L. H. Stephens, H. D. McClintock, J. Y. Sim and I. Y. Wong, Stereolithographic printing of ionically-crosslinked alginate hydrogels for degradable biomaterials and microfluidics, *Lab Chip*, 2017, **17**(20), 3474–3488.

27 Z. Chen, T. Klein, R. Z. Murray, R. Crawford, J. Chang, C. Wu and Y. Xiao, Osteoimmunomodulation for the development of advanced bone biomaterials, *Mater. Today*, 2016, **19**(6), 304–321.

28 Z. Chen, A. Bachhuka, S. Han, F. Wei, S. Lu, R. M. Visalakshan, K. Vasilev and Y. Xiao, Correction to "Tuning Chemistry and Topography of Nanoengineered Surfaces to Manipulate Immune Response for Bone Regeneration Applications", *ACS Nano*, 2019, **13**(3), 3739–3739.

29 Z. Chen, S. Ni, S. Han, R. Crawford, S. Lu, F. Wei, J. Chang, C. Wu and Y. Xiao, Nanoporous microstructures mediate osteogenesis by modulating the osteo-immune response of macrophages, *Nanoscale*, 2017, **9**(2), 706–718.

30 Q. Ou, K. Huang, C. Fu, C. Huang, Y. Fang, Z. Gu, J. Wu and Y. Wang, Nanosilver-incorporated halloysite nanotubes/gelatin methacrylate hybrid hydrogel with osteoimmunomodulatory and antibacterial activity for bone regeneration, *Chem. Eng. J.*, 2020, **382**, 123019.

31 C. Li, L. Yang, X. Ren, M. Lin, X. Jiang, D. Shen, T. Xu, J. Ren, L. Huang and W. Qing, Groove structure of porous hydroxyapatite scaffolds (HAS) modulates immune environment via regulating macrophages and subsequently enhances osteogenesis, *JBIC, J. Biol. Inorg. Chem.*, 2019, **24**(5), 733–745.

32 D. Karazisis, A. M. Ballo, S. Petronis, H. Agheli, L. Emanuelsson, P. Thomsen and O. Omar, The role of well-defined nanotopography of titanium implants on osseointegration: cellular and molecular events in vivo, *Int. J. Nanomed.*, 2016, **11**, 1367–1382.

33 S. Zhang, B. Ma, F. Liu, J. Duan, S. Wang, J. Qiu, D. Li, Y. Sang, C. Liu, D. Liu and H. Liu, Polylactic Acid Nanopillar Array-Driven Osteogenic Differentiation of Human Adipose-Derived Stem Cells Determined by Pillar Diameter, *Nano Lett.*, 2018, **18**(4), 2243–2253.

34 M. Nouri-Goushki, L. Angeloni, K. Modaresifar, M. Minneboo, P. Boukany, M. J. Mirzaali, L. E. Fratila-Apachitei and A. A. Zadpoor, 3D printed submicron patterns reveal the interrelation between cell adhesion, cell mechanics, and osteogenesis, *ACS Appl. Mater. Interfaces*, 2021, In Press.

35 J. M. Daley, J. S. Reichner, E. J. Mahoney, L. Manfield, W. L. Henry, B. Mastrofrancesco and J. E. Albina, Modulation of macrophage phenotype by soluble product (s) released from neutrophils, *J. Immunol.*, 2005, **174**(4), 2265–2272.

36 L. C. Borish and J. W. Steinke, 2. Cytokines and chemokines, *J. Allergy Clin. Immunol.*, 2003, **111**(2, Supplement 2), S460–S475.

37 K. Yang, Y. Wu, H. Xie, M. Li, S. Ming, L. Li, M. Li, M. Wu, S. Gong and X. Huang, Macrophage-mediated inflammatory response decreases mycobacterial survival in mouse MSCs by augmenting NO production, *Sci. Rep.*, 2016, **6**(1), 27326.

38 Y. Bi, J. Chen, F. Hu, J. Liu, M. Li and L. Zhao, M2 Macrophages as a Potential Target for Antiatherosclerosis Treatment, *Neural Plast.*, 2019, **2019**, 6724903.

39 A. C. La Flamme, M. Kharkrang, S. Stone, S. Mirmoeini, D. Chuluundorj and R. Kyle, Type II-activated murine macrophages produce IL-4, *PLoS One*, 2012, **7**(10), e46989–e46989.

40 L. Darwich, G. Coma, R. Peña, R. Bellido, E. J. J. Blanco, J. A. Este, F. E. Borras, B. Clotet, L. Ruiz, A. Rosell, F. Andreo, R. M. E. Parkhouse and M. Bofill, Secretion of interferon-gamma by human macrophages demonstrated at the single-cell level after costimulation with interleukin (IL)-12 plus IL-18, *Immunology*, 2009, **126**(3), 386–393.

41 J. Wang, Y. Su, L. Xu and D. Li, Micro-patterned surface construction on BCP ceramics and the regulation on inflammation-involved osteogenic differentiation, *Mater. Sci. Eng., C*, 2020, **116**, 111220.

42 M. Weber, A. B. Mackenzie, S. D. Bull and T. D. James, Fluorescence-Based Tool To Detect Endogenous Peroxynitrite in M1-Polarized Murine J774.2 Macrophages, *Anal. Chem.*, 2018, **90**(17), 10621–10627.

43 L. Lv, Y. Xie, K. Li, T. Hu, X. Lu, Y. Cao and X. Zheng, Unveiling the Mechanism of Surface Hydrophilicity-Modulated Macrophage Polarization, *Adv. Healthcare Mater.*, 2018, **7**(19), 1800675.

44 S. Gao, R. Lu, X. Wang, J. Chou, N. Wang, X. Huai, C. Wang, Y. Zhao and S. Chen, Immune response of macrophages on super-hydrophilic TiO_2 nanotube arrays, *J. Biomater. Appl.*, 2020, **34**(9), 1239–1253.

45 K. Garg, N. A. Pullen, C. A. Oskeritzian, J. J. Ryan and G. L. Bowlin, Macrophage functional polarization (M1/M2) in response to varying fiber and pore dimensions of electrospun scaffolds, *Biomaterials*, 2013, **34**(18), 4439–4451.

46 E. Lamers, X. F. Walboomers, M. Domanski, L. Prodanov, J. Melis, R. Luttge, L. Winnubst, J. M. Anderson, H. J. G. E. Gardeniers and J. A. Jansen, In vitro and in vivo evaluation of the inflammatory response to nanoscale grooved substrates, *Nanomedicine*, 2012, **8**(3), 308–317.

47 S. Dobbenga, L. E. Fratila-Apachitei and A. A. Zadpoor, Nanopattern-induced osteogenic differentiation of stem cells – A systematic review, *Acta Biomater.*, 2016, **46**, 3–14.

48 F. Y. McWhorter, T. Wang, P. Nguyen, T. Chung and W. F. Liu, Modulation of macrophage phenotype by cell

shape, *Proc. Natl. Acad. Sci. U. S. A.*, 2013, **110**(43), 17253–17258.

49 S. F. B. Mennens, K. van den Dries and A. Cambi, Role for Mechanotransduction in Macrophage and Dendritic Cell Immunobiology, in *Macrophages: Origin, Functions and Biointervention*, ed. M. Kloc, Springer International Publishing, Cham, 2017, pp. 209–242.

50 S. Wan, X. Fu, Y. Ji, M. Li, X. Shi and Y. Wang, FAK- and YAP/TAZ dependent mechanotransduction pathways are required for enhanced immunomodulatory properties of adipose-derived mesenchymal stem cells induced by aligned fibrous scaffolds, *Biomaterials*, 2018, **171**, 107–117.

51 Z. Geng, Z. Li, Z. Cui, J. Wang, X. Yang and C. Liu, Novel Bionic Topography with MiR-21 Coating for Improving Bone-Implant Integration through Regulating Cell Adhesion and Angiogenesis, *Nano Lett.*, 2020, **20**(10), 7716–7721.

52 F. Melo-Fonseca, G. Miranda, H. S. Domingues, I. M. Pinto, M. Gasik and F. S. Silva, Reengineering Bone-Implant Interfaces for Improved Mechanotransduction and Clinical Outcomes, *Stem Cell Rev. Rep.*, 2020, **16**(6), 1121–1138.

53 E. N. Schaumann and B. Tian, Actin-packed topography: Cytoskeletal response to curvature, *Proc. Natl. Acad. Sci. U. S. A.*, 2019, **116**(46), 22897–22898.

54 C.-H. Lee, Y.-J. Kim, J.-H. Jang and J.-W. Park, Modulating macrophage polarization with divalent cations in nanostructured titanium implant surfaces, *Nanotechnology*, 2016, **27**(8), 085101.

55 M. Shi, W. Song, T. Han, B. Chang, G. Li, J. Jin and Y. Zhang, Role of the unfolded protein response in topography-induced osteogenic differentiation in rat bone marrow mesenchymal stem cells, *Acta Biomater.*, 2017, **54**, 175–185.

56 I. Cockerill, Y. Su, J. H. Lee, D. Berman, M. L. Young, Y. Zheng and D. Zhu, Micro-/Nanotopography on Bioresorbable Zinc Dictates Cytocompatibility, Bone Cell Differentiation, and Macrophage Polarization, *Nano Lett.*, 2020, **20**(6), 4594–4602.

57 M. J. Vassey, G. P. Figueredo, D. J. Scurr, A. S. Vasilevich, S. Vermeulen, A. Carlier, J. Luckett, N. R. M. Beijer, P. Williams, D. A. Winkler, J. de Boer, A. M. Ghaemmaghami and M. R. Alexander, Immune Modulation by Design: Using Topography to Control Human Monocyte Attachment and Macrophage Differentiation, *Adv. Sci.*, 2020, **7**(11), 1903392.

58 M. Li, X. Fu, H. Gao, Y. Ji, J. Li and Y. Wang, Regulation of an osteon-like concentric microgrooved surface on osteogenesis and osteoclastogenesis, *Biomaterials*, 2019, **216**, 119269.